17th World Conference on Earthquake Engineering, 17WCEE
Sendai, Japan - September 13th to 18th 2020

EXPERIMENTAL STUDY ON BRB STABILITY WITH FLEXURAL-DEFORMED RESTRAINER

A.C. Wu(1), I.C. Ou(2), L.W. Chen(2), K. C. Tsai(3)

(1) *Associate Researcher, National Center for Research on Earthquake Engineering, Taipei, Taiwan, acwu@ncree.narl.org.tw*
(2) *Graduate research assistant, Department of Civil Engineering, National Taiwan University, Taipei, Taiwan*
(3) *Professor, Department of Civil Engineering, National Taiwan University, Taipei, Taiwan, kctsai@ntu.edu.tw*

Abstract

Researches on buckling-restrained braces (BRBs) have indicated the gusset rotational stiffness, strength and the BRB global stability are very critical to the expected seismic performance of buckling-restrained braced frames (BRBFs). Two BRB out-of-plane (OOP) stability assessment procedures have been developed recently by others. However, they either were not valid for the welded-end BRBs commonly used in Taiwan or required enormous calculating demands. This study develops a simplified analytical model using the concept of the notional load and considering the flexural restrainer to assess the BRB global stability. Cyclic loading tests on four full-scale BRBs of a yield strength of about 988 kN with varying restrainer stiffness, gusset thickness and with/without edge stiffeners or OOP end drift were conducted to demonstrate the effectiveness of the proposed method. Test results confirm that the effects of the initial imperfection, OOP drift, and gusset edge stiffener on the BRB and gusset global buckling strength can be satisfactorily predicted using the proposed method.

Keywords: buckling-restrained brace; global stability; flexural restrainer; notional load; buckling mechanism

1. Introduction

Buckling-restrained braces (BRB) have been widely recognized as cost-effective energy dissipaters for seismic-designed buildings around the world in the past few decades. Studies have confirmed that buckling-restrained braced frames (BRBF) possess high stiffness, strength, and seismic resilience. However, issues of BRB out-of-plane (OOP) instability, mitigating the aforementioned benefits, have been documented [1, 2]. As a result, the stability of BRBs has become a critical issue in BRBF design and applications. Several studies have been conducted recently to establish stability criteria for BRBs in order to ensure stable performance. Matsui et al. [3] highlighted the importance of the rotational strength, or the moment transfer capacity, at the restrainer end that dramatically affects the overall stability of BRBs. Takeuchi et al. [4, 5] proposed an advanced stability model based on the observation in which the overall instability is triggered by plastic hinges formed during compressive loading. Meanwhile, it considers initial imperfection, OOP end drift, flexural connection and rigid restrainer. Nevertheless, the collapse mechanisms illustrated in Takeuchi's models involve the un-deformed restrainer, which is inconsistent with the buckling mode observed in the previous frame test [2]. Zaboli et al. [6] adopted the notional load yielding line method and proposed a simplified method to determine the minimum size of gusset plates required to achieve overall OOP stability for both BRBFs and concentrically braced frames. Again, this method is developed based on the collapse mechanisms of Takeuchi's models, which neglects the buckling mode with flexural deformed restrainer.

This study introduces an analytical model for OOP stability assessment [7] of welded-end BRBs using the notional load yield-line method [6] and considering the restrainer flexibility. In order to verify the effectiveness of the proposed model, four full-scale welded-end BRB specimens with different restrainer stiffness, gusset thickness, and with/without gusset stiffeners or OOP end drift were adopted in the experimental program. All the specimens were designed to have the same nominal yield capacity of 988 kN and tested using the Multi-Axial Testing System (MATS) at National Center for Research on Earthquake

Engineering (NCREE) in Taiwan. It is demonstrated that the proposed method is able to satisfactorily predict the overall buckling strengths of the specimens.

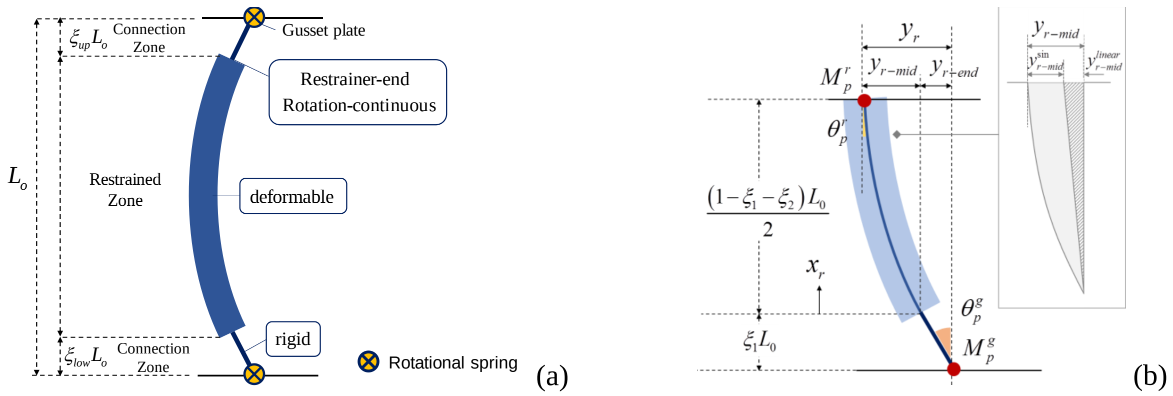

Fig. 1 – (a) Simplified collapse mechanism and (b) OOP deformations of the proposed model

2. Stability Assessment

According to the buckling mechanism observed in the frame test [2], the first-story BRB buckled in a symmetrical mode with gusset rotations and flexural deformed restrainer, while the restrainer ends and the connections remained undamaged. It features with that the bending flexibility of the restrainer is relatively significant compared with that of the connections for a welded-end BRB. In this study, the BRB assembly including gusset connections is simplified into two rotational hinges at both gussets and three members, both connection zones and a restrained zone, in series (Fig. 1a). Based on the test observations [8], the hinges are located on the BRB centerline twice the gusset thickness away from the BRB end. Given the fact that the rotational stiffness at the restrainer end is significantly higher than that at the gusset, the curvature at the restrainer end is assumed as continuous without rotation effect. The restrainer flexibility and a symmetrical buckling mode induced by the gussets rotations with rigid connection zones are considered to illustrate the behavior of a welded-end BRB in compression.

In the proposed model, at least two plastic hinges forming at both gussets along with flexural deformed restrainer are required for the system collapse. If the system continues to be loaded, the plastic moment strength would be developed at the mid-span of the restrainer to mature an additional plastic hinge. According to the symmetrical buckling shape, the maximum OOP deformation (y_r), including the terms of $y_{r\text{-}mid}$ and $y_{r\text{-}end}$, is developed at the mid-span of the restrainer as shown in Fig. 1b. In order to formulate the flexural restrainer, the distribution of OOP deformation $y_{r\text{-}mid}$ is defined as the superposition of a sine ($y_{r-mid}^{\sin}$) and a linear (y_{r-mid}^{linear}) functions:

$$y_r(x_r) = y_{r-mid}(x_r) + y_{r-end} = \left[y_{r-mid}^{\sin} \sin\left(\frac{\pi x_r}{(1-\xi_1-\xi_2)L_0} \right) + y_{r-mid}^{linear} \frac{x_r}{(1-\xi_1-\xi_2)L_0/2} \right] + y_{r-end} \tag{1}$$

where x_r is original from the restrainer end to its mid-span; $y_{r\text{-}mid}$ is the OOP deformation starting from the restrainer end; $y_{r\text{-}end}$ is the OOP deformation at the restrainer end; L_0 is the model effective length between the two rotational hinges; ξ_1 and ξ_2 are ratios of the connection zone lengths to L_0. The rotation angels of the plastic hinges at the gussets (θ_p^g) and the restrainer mid-span (θ_p^r) can then be expressed as:

$$\theta_p^g = \left.\frac{dy_r(x_r)}{dx_r}\right|_{x_r=0} = y_{r-mid}^{\sin} \frac{\pi}{(1-\xi_1-\xi_2)L_0} + y_{r-mid}^{linear} \frac{1}{(1-\xi_1-\xi_2)L_0/2} = \frac{y_{r-end}}{\xi_1 L_0} \tag{2}$$

$$\theta_p^r = \left.\frac{dy_r(x_r)}{dx_r}\right|_{x_r=\frac{(1-\xi_1-\xi_2)L_0}{2}} = y_{r-mid}^{linear} \frac{1}{(1-\xi_1-\xi_2)L_0/2} \tag{3}$$

Using the system of Eqs. (1) and (2), the OOP deformation components from the sine and linear effects can be resolved as:

$$y_{r-mid}^{\sin}=\left(\frac{y_{r-end}}{\xi_1 L_0}-\frac{y_{r-mid}}{(1-\xi_1-\xi_2)L_0/2}\right)\Bigg/\frac{\pi-2}{(1-\xi_1-\xi_2)L_0} \tag{4}$$

$$y_{r-mid}^{linear}=\left(\frac{\pi y_{r-mid}}{(1-\xi_1-\xi_2)L_0}-\frac{y_{r-end}}{\xi_1 L_0}\right)\Bigg/\frac{\pi-2}{(1-\xi_1-\xi_2)L_0} \tag{5}$$

As shown in Eq. (3), the development of the plastic hinge at the restrainer mid-span is represented by the term of y_{r-mid}^{linear}, while the $y_{r-mid}^{\sin}$ term shows the restrainer flexibility. In this study, the concept of the notional load is adopted to quantify the second-order effect of initial imperfection. As shown in Fig. 2a, the total initial imperfection of θ_i in a BRB assembly, including the plumbing tolerance of the brace, out-of-flatness tolerance of the gusset, restrainer-to-core clearance, and load eccentricity, is assumed as a combination of fabrication error a_0 at the restrainer mid-span and the initial OOP end drift δ_0 as:

$$\theta_i=\frac{a_0}{L_0/2}+\frac{\delta_0}{L_0} \tag{6}$$

The notional load at the brace end and restrainer mid-span shown in Fig. 2b is equivalent to

$$N=P\theta_i \tag{7}$$

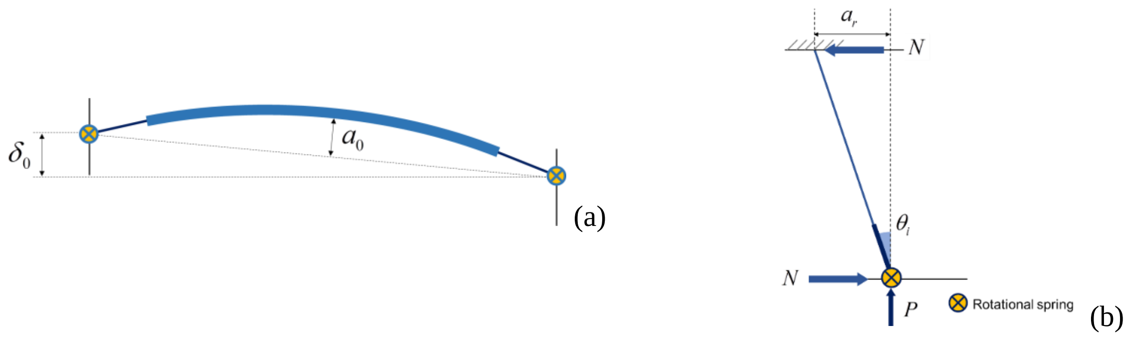

Fig. 2 – (a) Initial imperfection and OOP drift, and (b) concept of lateral notional load

According to the virtual work principle, the BRB global stability condition is expressed as energy equilibrium of the external work made by the notional load and the internal energy consumed by the flexural deformed restrainer and plastic hinges under the expected failure mechanism.

$$N\delta_s y_r\le\int_0^{\frac{(1-\xi_1-\xi_2)L_0}{2}}\frac{EI_{eff}}{2}\left(\frac{d^2y_r(x_r)}{dx_r^{\,2}}\right)^2dx_r+M_p^r\theta_p^r+M_p^g\theta_p^g \tag{8}$$

Thus, the stability limit can be determined using the following expression:

$$P\theta_i\delta_s y_r\le\frac{\pi^4EI_{eff}}{8\left((1-\xi_1-\xi_2)L_0\right)^3}\left(y_{r-mid}^{\sin}\right)^2+M_p^r\theta_p^r+M_p^g\theta_p^g \tag{9}$$

where δ_s is the moment amplification factor; EI_{eff} is the restrainer's effective bending rigidity; M_p^r is the restrainer plastic moment capacity; M_p^g is the reduced gusset plastic moment capacity including axial force effect. The predicted buckling strength calculated from Eq. (9) is defined as P_{lim}. More details about the second-order effect, elastic buckling capacity, restrainer, and gusset moment capacities required for the assessment procedure can be found [7].

3. Experimental Program

3.1 Specimen Design

The specimens were designed to reflect a typical BRBF with a beam bay width of 6000 mm and a story height of 4000 mm. The beam depth is 500 mm and the column width is 550 mm. These four specimens were constructed using CNS SN490B steel (nominal yielding strength σ_{cy} = 325 MPa) with the same core cross-sectional properties and longitudinal dimensions. Thus, the four specimens have the same design yield strength. The detailed dimensions are illustrated in Fig. 3 and given in Table 1. The specimens were denoted such that the first three alphanumeric letters indicate the thickness of the gusset. The label 'LC' denotes a larger restrainer, while 'ES' denotes the gusset stiffeners. The maximum possible compressive strength, P_{max}, was estimated to be 1772 kN from the nominal yielding strength and the suggested adjustment factors for SN490B steel. These factors include the material over-strength (1.2), strain hardening (1.3), and compression strength adjustment (1.15) factors. The specimens were fabricated using 16-mm- or 18-mm-thick gussets (G16 or G18). In order to understand the restrainer's flexural effects, one of the BRBs' restrainers was made from a larger casing (G18_LC) 267 mm in diameter. One of the BRB specimens (G16_ES) was equipped with 10-mm-thick stiffeners along the long sides of its gussets to investigate the effects of the gusset stiffener. The detailed designs were based on existing procedures [9], in which the stability demand-to-capacity ratio (DCR) of the steel casing, connections, and gussets were checked separately. The BRB's compressive force demand of 1772 kN was applied in computing these DCRs.

Table 1 – Dimensions and strengths of specimen

ID	B_c (mm)	t_c (mm)	B_j (mm)	D_j (mm)	R_r (mm)	t_r (mm)	t_g (mm)	L_c (mm)	L_t (mm)	L_j (mm)	L_{sc} (mm)	L_{BRB} (mm)
G18	103	16	162	172	216.3	7	18	4530	70	1270.5	5210	5760
G16					216.3		16					
G18_LC					267.4		18					
G16_ES					216.3		16					

Table 2 – Designed stability results (DCRs) for individual limit state

Limit state	G18	G16	G18_LC	G16_ES
BRB steel casing flexural buckling	0.97	0.97	0.58	0.97
BRB connection region compression buckling	0.90	0.90	0.90	0.90
Gusset plate compression buckling [K=0.65]	0.83	1.05	0.83	1.05
[K=2.0]	1.10	1.34	1.10	1.34

The evaluation results are given in Table 2. These calculations did not consider the strength reduction factor. Specimens with a 216.3 mm restrainer (G18, G16, G16_ES) all have a rather critical DCR value of 0.97 in the steel casing flexural buckling check. In contrast, G18_LC, which equipped with a 267.4 mm restrainer, has a quite low DCR value of 0.58. G18_LC was supposed to be designed with a restrainer of which the diameter is in between 216.3 mm and 267.4 mm, possibly with a DCR of about 0.8 so that there would be a more striking comparison to justify the effectiveness of this method. However, the restrainer selection depended on whether the manufacturer had the steel casing with needed size in stock. Therefore, it was actually an expediency to make such restrainer layouts. It is noted that an effective length factor (K) of 0.65 is adopted in calculating the gusset's compression buckling strength when the edge stiffeners are detailed. On the other hand, a value of K = 2.0 is applied for the case without them. The DCRs for the four specimens calculated using the K values described above are listed in Table 2. However, the evaluation results of using both the K values on all four specimens are also listed in Table 2 for comparison purposes. G16 has a DCR of 1.34 in the gusset compression buckling check, indicating an unsafe design, while G18, G18_LC, and

G16_ES have smaller DCRs, but still greater than 1.0. To sum up, based on these limit state evaluation results, the four specimens were designed to have various levels of gusset buckling potential.

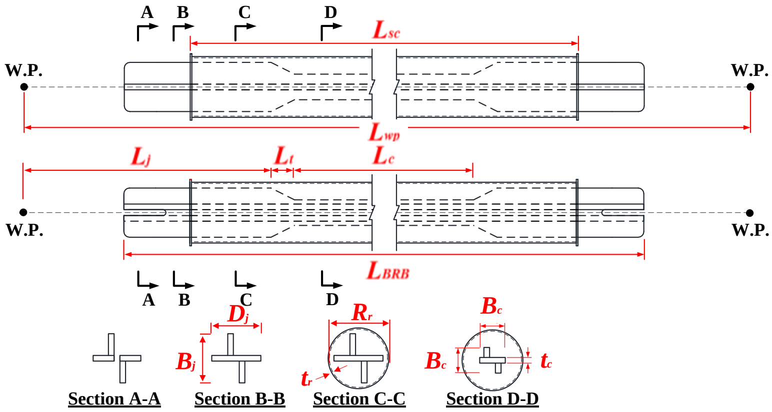

Fig. 3 – Detailed dimensions of the specimens

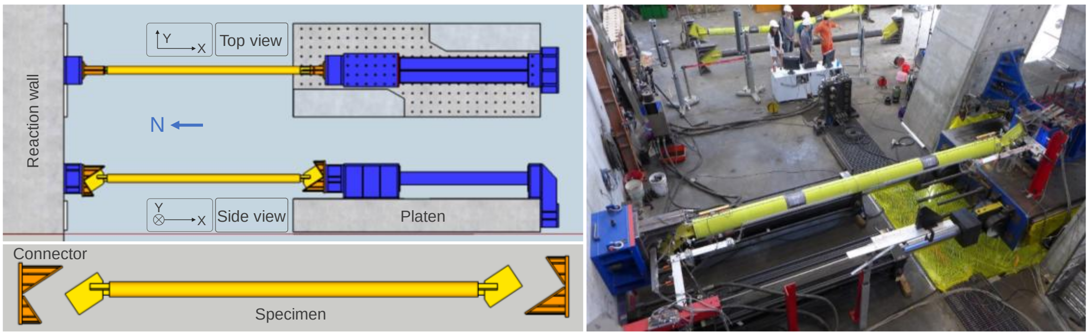

Fig. 4 – Test setup

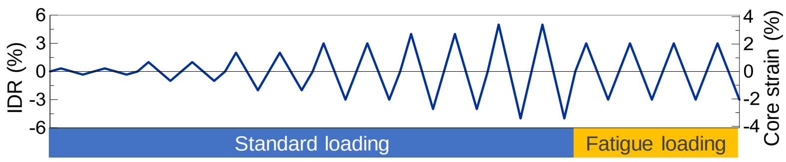

Fig. 5 – Loading protocol

3.2 Test Setup and Procedure

Figure 4 illustrates the test setup, where the positive X-direction is toward the south (the platen side), and the positive Y-direction is toward the east. This coordinate system was applied for both the loading protocol and the instrumentation. Two gusset connectors were fabricated to provide end boundary conditions for the gussets, and to simulate the gusset-to-beam and gusset-to-column interfaces. It should be noted that both the in-plane and OOP rotation of the beam–column joint is neglected in this study. Thus, the gusset connectors were stiffened to be sufficiently rigid without in-plane rotation. In order to recover the OOP deformations of the specimens, an optical measuring system (OMS), which comprise a controller, a camera and several markers, was used.

The specimens were tested by applying cyclically increasing displacements. The loading protocol comprised the standard and fatigue cyclic loading tests, as illustrated in Fig. 5. The standard loading cycles followed the recommendations of AISC 341-10 [10] for BRBs, where the first two cycles consider the yielding displacement of the BRB specimen. Then, the loading proceeds with an increasing IDR ranging from 1% to 4% for two cycles at each level. In order to trigger the instability of the specimens, two additional cycles with a 5% IDR were adopted following the last cycle of 4% IDR if necessary. Once the specimen went through the abovementioned loading cycles without failure, the fatigue cyclic loading test with constant displacements of 3% IDR was repeated until failure occurred.

3.3 Test results

G18, G16, and G16_ES buckled with plastic hinges forming at the gussets and significant flexural deformation developing along their restrainers, as shown in Figs. 6 to 8. G18_LC exhibited a stable performance throughout the loading cycles without any observable damage. Fatigue failure did occur at the 16th cycle in the subsequent fatigue test. The BRB force vs. axial deformation relationships are given in Fig. 9 for all specimens.

 (a) 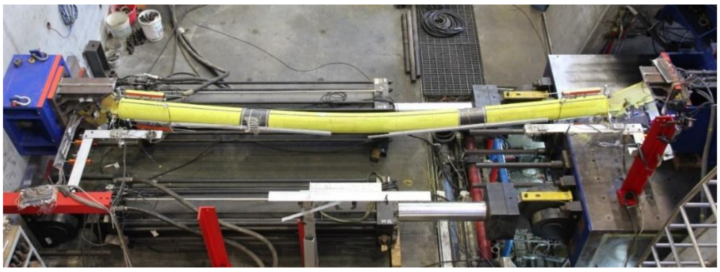 (b)

Fig. 6 – (a) The folding line at the southern gusset and (b) the buckling shape of G18

Specimen G18

G18 buckled at the first cycle of 5% IDR and the axial strength dropped drastically after reaching 2118 kN. The maximum tensile strength was 1728 kN at the peak of 5% IDR. The compressive strength adjustment factor, β, was computed to be 1.17 from the second cycle of 4% IDR. The cumulative plastic deformation (CPD) had reached 252 by the time it buckled. An OOP end drift of 7.3 mm was measured by the OMS. From the axial force vs. axial deformation relationships, it can be seen that the axial stiffness rose slightly during compression in the 4% IDR cycles, and even went higher during the 5% IDR cycle. This kind of phenomenon was also observed in the other specimens, which should be caused by the effects of severe high-mode buckling developed along the core. Fig. 6a shows the folding line developed on the gussets when the global instability occurred. The overlap portion between the gusset and the joint segment formed a rigid zone, which pushed the folding line inward to the gussets, causing a curved folding line. The distance between the end of the BRB member and the folding line is approximately twice the gusset thickness.

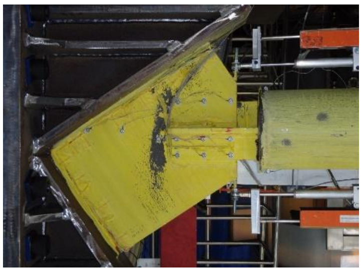 (a)  (b)

Fig. 7 – (a) The folding line at the southern gusset and (b) the buckling shape of G16

Specimen G16

G16 buckled during the first 3% IDR loading cycle with an initial OOP end drift of 57.4 mm caused by experimental misalignment. The buckling strength was 1721 kN, while the maximum tensile strength was 1607 kN. The β value was 1.11, calculated from the second cycle of 2% IDR. By the time it buckled, the

CPD had reached over 80. After buckling, G16 was stretched first and compressed again. It can be seen that the BRB member somehow behaved like a conventional buckling brace and completely lost its stability even through it had been re-stretched. The axial force vs. axial deformation relationships are illustrated in the plot designated "G16_After buckling" in Fig. 9. Figure 7a shows the folding line developed on the gusset. Again, the distance between the end of the BRB member and the center of the folding line was twice the gusset thickness.

Specimen G18_LC

G18_LC exhibited stable hysteresis behavior throughout the standard cyclic loading test without any observable instability or damage. Subsequently, a fatigue cyclic loading test with a constant amplitude of 3% IDR proceeded. The core fatigue fracture did occur at the sixteenth cycle of the fatigue test. The total CPD reached over 674 at the end of the tests. The maximum tensile strength and the maximum compressive strength developed at the second cycle of 5% IDR were 1747 kN and 2178 kN, respectively. The corresponding β value was 1.25. A large end drift of 72.2 mm was measured at the initial state and was attributed to experimental misalignment.


(a)

(b)

Fig. 8 – The folding line at the southern gusset and (b) the buckling shape of G16_ES

Specimen G16_ES

Concerning the unintentional OOP end drift measured from the abovementioned tests, G16_ES was carefully calibrated without any drift in the first place using the OMS. G16_ES performed stably throughout the prescribed standard loading cycles without any observable damage. Thus, it was further subjected to an OOP end drift of L_0/100 (57.1 mm) and loaded from the 3% IDR cycle to investigate the effects of end drift on the overall stability. Eventually, G16_ES buckled at the first cycle of 5% IDR with a buckling strength of 1942 kN. The maximum tensile strength was 1680 kN. The β value was 1.16, as calculated from the second cycle of 4% IDR with the end drift. The CPD reached 491. Figure 8a shows the folding line developed on the gusset. It can be found that the edge stiffener welded along the long side of the gusset had impeded the development of the folding line near the gusset's free edges, causing a more curved folding line. The axial force vs. axial deformation relationships with no end drift and with end drift, designated as "G16_ES(I)" and "G16_ES(II)", respectively, are given in Fig. 9.

4. Conclusions

Existing methods do not consider either the coupling effects of the gussets' and the restrainer's buckling, or the effects of the restrainer's flexural deformation. Therefore, these methods may lead to incorrect predictions of the buckling mode and strength. The proposed model considers both the aforementioned coupling effects and the restrainer's flexural deformation. It is able to provide a more reliable design for welded-end BRBs (Table 3) and gusset connections compared to that given by existing methods.

Three specimens buckled with severe OOP deformations of the restrainer and plastic hinges forming at the gussets. The restrainer's flexural stiffness plays a critical role with respect to the overall BRB stability. The test results for G16, G16_ES(II), and G18 confirmed that the improvement in the overall stability is limited when attaching only one gusset stiffener or using slightly thicker gussets. Doubling the gusset's rotational stiffness and strength from G16 to G16_ES(II) improves the buckling strength by only 13%. The test results for G16_ES(I) and G16_ES(II) confirmed that a large OOP end drift can trigger severe OOP deformation and subsequent buckling. An end drift of L_0/100 in G16_ES(II) reduced the buckling strength by at least 9%, indicating that the OOP end drift is a crucial factor affecting the overall stability.

Table 3 – Stability evaluation results

Specimen	IDR	a_0 (mm)	δ_0 (mm)	P_{lim} (kN)	P_{exp} (kN)	$(P_{lim}-P_{exp})/P_{exp}$	P_{exp}/P_{lim}
G18	5.0%	7.6	7.3	2187	2118	3.3%	0.97
G16	3.0%	9.0	57.4	1681	1721	-2.3%	1.02
G18LC	5.0%	16.3	72.7	3646	2178*	-	0.60
G16ES (I)	5.0%	21.0	0.3	2263	2126*	-	0.94
G16ES (II)	5.0%		57.1	1852	1942	-4.6%	1.05

*Peak compressive strength of stable specimens measured during the loading cycle.

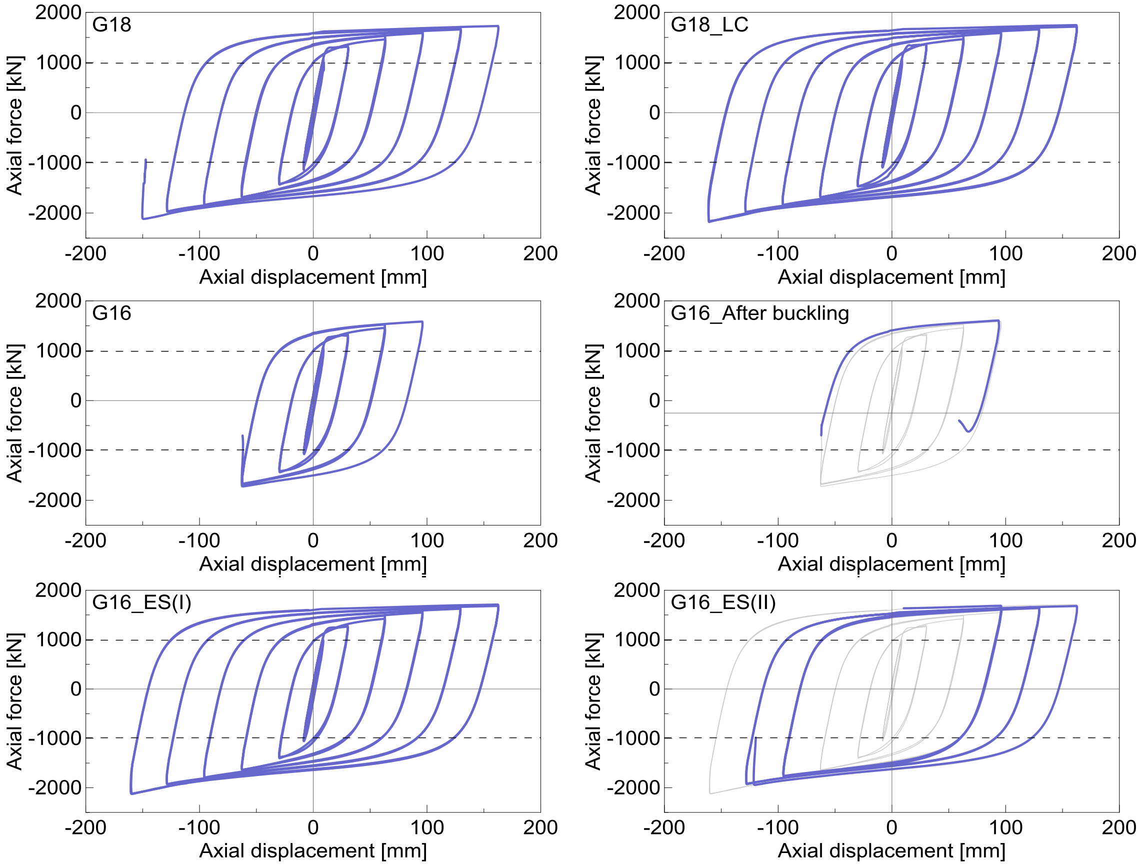

Fig. 9 – Hysteresis loops of the specimens

6. References

[1] Tsai KC, Hsiao PC (2008): Pseudo-dynamic tests of a full-scale CFT/BRB frame -Part II: Seismic performance of buckling restrained braces and connections. *Earthquake Engineering & Structural Dynamics*, **37** (7): 1099-1115.

[2] Wu AC, Tsai KC, Yang HH, Huang JL, Li CY, Wang KJ, Khoo HH (2016): Hybrid experimental performance of a full-scale two-story buckling-restrained braced RC frame. *Earthquake Engineering & Structural Dynamics*, **46** (8): 1223-1244.

[3] Matsui R, Takeuchi T, Nishimoto K, Takahashi S, Ohyama T (2010): Effective buckling length of buckling-restrained brace considering rotational stiffness at restrainer ends. *7th International Conference on Urban Earthquake Engineering & the 5th International Conference on Earthquake Engineering Proceedings*, Tokyo, Japan.

[4] Takeuchi T, Ozaki H, Matsui R, Sutcu F (2014): Out-of-plane stability of buckling-restrained brace including moment transfer capacity. *Earthquake Engineering & Structural Dynamics*, **43** (6): 851-869.

[5] Takeuchi T, Ozaki H, Matsui R, Sutcu F (2016): Out-of-plane stability assessment of buckling-restrained brace including connections with chevron configuration. *Earthquake Engineering & Structural Dynamics*, **45** (12): 1895-1917.

[6] Zaboli B, Clifton C, Cowie K (2017): Out-of-plane stability of gusset plates using a simplified notional load yield line method. *NZSEE Annual Technical Conference and the 15th World Conference on Seismic Isolation, Energy Dissipation and Active Vibration Control of Structures*, Wellington, New Zealand.

[7] Ou IC (2018): A study of global out-of-plane stability model for BRBs using notional load and plastic analysis. *Master Thesis*, Department of Civil Engineering, Nation Taiwan University, Taipei, Taiwan.

[8] Chen LW, Tsai KC, Tsai CY, Wu AC (2019): Evaluating out-of-plane stability for welded BRBs considering flexural restrainer and gusset rotations. *Journal of Constructional Steel Research*, **159**: 161-175.

[9] Chuang MC, Tsai KC, Lin PC, Wu AC (2015): Critical limit states in seismic buckling-restrained brace and connection designs. *Earthquake Engineering and Structural Dynamics*, **44** (10): 1559-1579.

[10] American Institute of Steel Construction (2010): *Seismic Provisions for Structural Steel Buildings (AISC 341-10)*. AISC, Chicago, Illinois.

